Cellular Oncology (2025) 48:1693–1710
https://doi.org/10.1007/s13402-025-01093-2

RESEARCH

Unraveling the miR-144-3p/PUMA pathway: a novel regulator of FDX1-mediated cuproptosis in colorectal cancer

Guiyun Jia[1,3] · Jiehan Li[3,4] · Meimei Jiang[1,3] · Nannan Liu[1,3] · Ning Ding[1,3] · Xinxiu Jiang[3] · Ge Zhang[3,4] · Xiaoxiao Tan[3] · Ying Kang[3] · Lingling Zhang[3] · Feng Wang[1,2] · Yingjie Zhang[1,3]

Received: 16 April 2025 / Accepted: 16 July 2025 / Published online: 10 November 2025

Abstract

Purpose Cuproptosis represents a novel form of cell death, predominantly driven by excessive intracellular accumulation of Cu^{+}. The mechanisms underlying cuproptosis in colorectal cancer (CRC) remain unknown. This study aims to investigate the underlying mechanisms in CRC, offering a novel therapeutic strategy for its treatment.

Methods Transcriptomic datasets from The Cancer Genome Atlas (TCGA) databases were analyzed using R-software (v4.3.1) to quantify miR-144-3p expression in CRC. In vitro, CCK-8, EdU, colony formation assays, and Transwell assays were used to assess the proliferative capacity, migratory potential, and invasive properties of CRC under miR-144-3p modulation. Western blotting (WB) further linked miR-144-3p expression to modulation of cuproptosis-related pathways. RNA immunoprecipitation (RIP) and dual-luciferase reporter assays were performed to validate miR-144-3p binding to the 3′-UTR of *PUMA* mRNA. Co-IP and Immunofluorescence (IF) assays confirmed PUMA-FDX1 binding. DLAT oligomerization was analyzed by WB and IF experiments. The ubiquitination level of FDX1 was detected via Co-IP. In vivo, tumor xenograft experiments using $HCT116^{OE-miR-144-3p}$ and $HCT116^{sh-miR-144-3p}$ cell lines were performed in nude mice.

Results In this study, miR-144-3p, a recently identified microRNA, was found to be aberrantly upregulated in CRC. It significantly promoted the proliferation, migration, and invasion of CRC both in vitro and in vivo. Mechanistically, miR-144-3p directly bound to the 3′-UTR of *PUMA* mRNA, thereby inhibiting PUMA expression and function, which restrained cell death. Furthermore, PUMA induces cuproptosis by enhancing the function of FDX1 through the directly binding with its R155 site, which promotes the oligomerization of lipoylated DLAT/DLST and reduces LIAS expression. In addition, we identified the way in which FDX1 is depleted in the process of cuproptosis: the binding between PUMA and FDX1 raised the ubiquitination level at the K182 site, leading to the further degradation of FDX1.

Conclusions Our findings delineate a miR-144-3p/PUMA regulatory axis controlling cuproptosis homeostasis in CRC. PUMA acts as a functional regulator of cuproptosis, activating copper-dependent cell death by binding FDX1, thereby enhancing DLAT/DLST oligomerization and suppressing LIAS expression. This axis may offer a promising new approach and target for the treatment of CRC.

Keywords CRC · Cuproptosis · PUMA · FDX1 · miR-144-3p

✉ Feng Wang
wolffeng2000@hotmail.com

✉ Yingjie Zhang
yingjiezhang@hnu.edu.cn

[1] Department of Gastroenterology, Huadong Hospital, Shanghai Medical College, Fudan University, Shanghai 200040, China

[2] Mental Health Center Affiliated to Shanghai University of Medicine & Health Sciences, Shanghai 201318, China

[3] School of Biomedical Sciences, Hunan University, Changsha, Hunan 410082, China

[4] Department of Gastrointestinal Surgery, The First Affiliated Hospital of Zhengzhou University, Zhengzhou 450052, China

1 Introduction

Colorectal cancer (CRC) is the third most common malignant tumor globally exhibiting a rising incidence rate-particularly among younger populations under 50, where rates increased annually in recent years [1]. According to the World Health Organization researches, CRC is now the second leading cause of cancer-related deaths worldwide, with an estimated 3.2 million new cases and 1.6 million deaths projected by 2040 [2]. CRC originates in the intestinal mucosa and is mainly treated through surgical resection, chemotherapy, targeted therapy, and immunotherapy [3]. However, many drawbacks in each treatment: surgery may damage healthy tissue and causes relevant postoperative recidivation, and chemotherapy drugs often lead to issues such as severe side effects and drug resistance [4]. Although the early screening of tumor significantly reduces the incidence and mortality rates, about 30% of diagnosed patients still experience metastasis, with poor prognosis [5]. Developing novel targets or therapies is an urgent need for the treatment of CRC.

Cuproptosis is a novel form of cell death triggered by the abnormal accumulation or toxicity of copper ions [6]. Copper, an essential trace metal, crucial for various biochemical processes under physiological conditions. Copper ions participate in redox reactions through electron transfer, playing a vital role in cellular respiration and oxidative defense [6, 7]. However, when copper ion levels become imbalanced and excess copper accumulates, it triggers oxidative stress and disruption of cellular processes, causing cell damage and death. Specifically, cuproptosis occurs when copper ions directly bind to the lipoylated components of the tricarboxylic acid cycle, forming cytotoxic aggregates that induce cell death [8]. Targeting cuproptosis might provide novel insight into the therapy of CRC.

MicroRNAs (miRNAs) are a family of non-coding RNAs encoded by endogenous genes, typically 20–24 nucleotides in length [9]. MiRNAs were first discovered by Lee et al. in *Caenorhabditis elegans* [10]. Since then, more miRNAs have been identified, and their biogenesis pathways have been elucidated, revealing their regulatory functions under various physiological and pathological conditions [9, 11]. MiRNAs are widely present in animals, plants, and viruses, which characterized by high conservation, temporal expression specificity, and tissue-specific expression [12]. MiRNAs recognize and bind to 2–7 nucleotide sequences in the 3' untranslated region (3′-UTR) of target mRNAs through imperfect base pairing, thereby interfering with the target mRNA [13]. MiRNAs primarily regulate gene expression post-transcriptionally by destabilizing target mRNAs and inhibiting their translation, which impacts tumor pathophysiology and distant metastasis and plays crucial roles in survival, proliferation, migration, and therapy resistance [14]. For instance, miR-21 is upregulated in various cancers, promoting tumor proliferation and inhibiting apoptosis [15], miR-223 regulates fibrosis as a key player [16], while miR-34 is considered a downstream regulator of the p53 pathway and is associated with tumor suppression [17]. And in CRC, many miRNAs have been reported to play pivotal roles in affecting immunoreaction [18], regulating liver metastasis [19] and regulating tumor growth [20].

PUMA (also known as BBC3) is a crucial apoptosis regulator and a member of the BCL-2 protein family, specifically classified as a BH3-only pro-apoptotic subtype [21]. Under various types of damage in cells, PUMA interacts with anti-apoptotic BCL-2 family members to inhibit their function, thereby promoting apoptosis [22]. Additionally, PUMA induces mitochondrial dysfunction by activating pro-apoptotic proteins such as BAX and BAK, leading to mitochondrial membrane permeabilization (MOMP). This releases apoptogenic factors, activating downstream apoptotic cascades that culminate in cell death [23]. Due to its ability to trigger apoptosis and eliminate damaged cells, PUMA plays a significant role in inhibiting tumor formation and progression. And whether miRNAs regulate PUMA function in cuproptosis is still unknown.

In the past few years, our team has focused on the investigation of the mechanisms underlying PUMA-mediated apoptosis [24–27] and the potential therapeutic applications of targeting PUMA [28, 29] in CRC. Building on the previous works, this study explores new functions of PUMA on the other cell death modes, and presents workflow in Fig. S1. Comprehensive analyses of public databases TCGA (https://www.cancer.gov/ccg/research/genome-sequencing/tcga), revealed that miR-144-3p is upregulated in CRC. Fu rther experimental results demonstrated that inhibiting the expression of miR-144-3p effectively suppressed malignant features of CRC. Mechanistically, miR-144-3p bound to the 3' -UTR of *PUMA* mRNA via partial base pairing, affecting its stability and inhibiting apoptosis. Additionally, we discovered that PUMA induces cuproptosis by directly binding to FDX1, thereby enhancing its function. Furthermore, the binding between PUMA and FDX1 raises the ubiquitination at the K182 site, leading to the further degradation of FDX1. The regulation of PUMA on cuproptosis offers a potential therapeutic target for CRC treatment.

2 Materials and methods

2.1 Cell lines and cell culture

Purchased HCT116 and SW620 human colorectal cancer cell lines, as well as Human Intestinal Epithelial Cells (HIEC), from the American Type Culture Collection (ATCC), all of which have been verified to be of good quality. The cells

were cultured in Dulbecco's Modified Eagle's Medium (DMEM, Gibco, USA) supplemented with 10% fetal bovine serum (FBS, Gibco, USA) at 37 °C with 5% CO_2. Perform cell transfection according to the instructions provided with the DNA transfection reagent (Neofect, China) and Lipofectamine 2000 (Thermo Fisher Scientific, USA).

2.2 Bioinformatic analysis from public database

MiRNA sequencing (miR-seq) data for COAD and READ were obtained from TCGA database using TCGAbiolinks (v2.26.0), comprising 633 samples. Raw count data were normalized using DESeq2's median-of-ratios method (v1.34.0) and subjected to differential expression analysis with thresholds of adj. p-value < 0.05 and|log-2-FC| >1. volcano plots and boxplots were performed using ggplot2 (v3.4.4) in R software (v4.3.1).

To determine CRCDEGs using GEO (https://www.ncbi.nlm.nih.gov/geo/) data (GEO-CRCDEGs), eight gene expression profile datasets (GSE77953, GSE44076, GSE41258, GSE113513, GSE103512, GSE44861, GSE39582, GSE20916, and GSE9750) from the GEO database were selected for analysis. The 8 datasets were divided into normal and colorectal cancer groups for analysis. The specific criteria for adjusted p-value < 0.05 were used to analyze DEGs with the "limma (V.3.54.0)" package. These differential genes were subjected to Venn analysis with TargetScan7.2_miR-144-3p_predicted_targets ($n = 147$) (https://www.targetscan.org/vert_72/) and Human.mitoCarta 3.0 (https://www.broadinstitute.org/files/shared/metabolism/mitocarta/human.mitocarta3.0.html) mitochondrial genes ($n = 1748$), showing one consensus target at the intersection.

All details of databases are in Supplementary Material 3.

2.3 RNA extraction and real-time quantitative polymerase chain reaction (qRT-PCR)

MiRNA was extracted from cells and tissues using the miRcute miRNA Extraction Kit (TIANGEN, China). Reverse transcription was performed using the miRcute Enhanced miRNA cDNA First-Strand Synthesis Kit (TIANGEN, China). QRT-PCR was conducted for miRNA with the miRcute Enhanced miRNA Fluorescence Quantification Detection Kit (TIANGEN, China) using the tailing method.

Total RNA was extracted using Trizol (TransGen Biotech, China), reverse transcribed with HiScript III All-in-One RT SuperMix Perfect (Vazyme, China). and qRT-PCR was carried out using ChamQ Universal SYBR qPCR Master Mix (Vazyme, China). All primer sequences were listed in Table 1. Data analysis was performed using the ΔΔCt method to compare relative RNA expression levels.

Table 1 The Details of primer sequences used in this study

Name	Sequence
Actin-F	TGGCACCCAGCACAATGAA
Actin-R	CTAAGTCATAGTCCGCCTAGAAGCA
PUMA-F	ACGACCTCAACGCGCAGTA
PUMA-R	CTAGTTGGGCTCCATTTCTGG
miR-144-3p-F	GCCGCCTACAGTATAGATGATGTACT
U6-F	AACGCTTCACGAATTTGCGT
U6-R	CTCGCTTCGGCAGCACA
3′-UTR Bing Site-F	GAGGGAGGAGTCTGGGAGT
3′-UTR Bing Site-R	CACTGTTCCAATCTGATTTTATTGAAAAGGA

2.4 Cell viability, colony formation assay, transwell assay and edu assay

The experimental procedures are based on the articles previously published by our research group [30–32].

2.5 Western blotting (WB)

Proteins from tissues and cells were extracted using RAPI lysis buffer (NCM Biotech, China), separated by 12% SDS-PAGE, and transferred to a 0.45 μm PVDF membrane (Millipore, Germany). The membrane was blocked with 5% non-fat milk (BioFroxx, Germany). The antibodies used in the experiment include anti-GAPDH (diluted at 1:3000), anti-Vimentin (diluted at 1:3000), anti-E-cadherin (diluted at 1:3000), anti-actin (diluted at 1:3000), anti-BAX (diluted at 1:1000), anti-BcL-2 (diluted at 1:1000), anti-caspase 3 (diluted at 1:1000), anti-cleaved caspase3 (diluted at 1:1000), anti-HA (diluted at 1:2000), anti-MYC (diluted at 1:2000), anti-His (diluted at 1:2000), anti-DLAT (diluted at 1:1500), anti-LIAS (diluted at 1:1000) and anti-Tubulin (diluted at 1:3000)from Proteintech, China, and anti-N-cadherin (diluted at 1:1000), anti-PUMA (diluted at 1:1000) and anti-FDX1 (diluted at 1:1000) from Abmart, China, and anti-DLST (diluted at 1:1000) from Solarbio, China.

2.6 RNA binding protein Immunoprecipitation assay (RIP)

Cross-linking proteins and RNA in cells was achieved using formaldehyde, and the RNA-protein complexes were incubated with anti-IgG (Beyotime, China) and anti-AgO2 (Proteintech, China) using the Magnetic RNA-Protein Pull-Down Kit (Thermo Fisher Scientific, USA). The RNA-silencing complexes were then pulled down, and the levels of PUMA sites in the pulled-down complexes were detected by qRT-PCR.

2.7 Dual-luciferase assay

Mut-PUMA (with binding site mutations) and MT-PUMA (without mutations) were constructed, then co-transfect them separately with miR-144-3p mimics. The interactions were analyzed using a dual-luciferase reporter assay kit (Beyotime, China) with a microplate reader.

2.8 Co-IP

Cells were lysed by Western and IP lysis buffer (Beyotime, China) and collected the protein-containing supernatants. Supernatants were divided into three parts: input, IgG, and IP. For the input, directly denature it; for the IgG group, add 1 µg of anti-IgG antibody; for the IP group, add the required antibody and then rotate at 4 °C overnight. The next day, add 40µL of Protein A+G Agarose (Beyotime, China) to both the IgG and IP groups and continue rotating at 4 °C for 4 h. After washing according to the instructions, denature the samples and perform Western blotting.

2.9 Cell flow cytometry

Cell apoptosis was assessed using the Apoptosis Detection Kit (4 A Biotech, China), and detection was performed with a BD flow cytometer.

2.10 ROS assay

Cells were treated with a Reactive Oxygen Species Detection kit (Solarbio, China), and observations were recorded using an inverted fluorescence microscope (Thermo, USA).

2.11 DNA damage comet assay

Cells were treated with a Comet Assay Kit (Beyotime, China), and observations were recorded using an inverted fluorescence microscope (Thermo, USA). At least 200 randomly selected single cells were then evaluated for % Tail DNA and Olive Tail Moment using the CASP_1.2.3b1.

2.12 Statistical analysis

The results were presented using GraphPad Prism 6.0 software after data processing Each experiment was independently repeated at least three times, and the presented results are representative of these repetitions. Data are expressed as mean ± standard deviation (SEM). Differences between two groups were calculated using the student's t-test. A p-value less than 0.05 was considered statistically significant.

3 Results

3.1 MiR-144-3p is upregulated in CRC and associated with tumor progression

The development of CRC is generally influenced by a variety of factors. To investigate the role of miRNA in the progression of CRC, we initially acquired miRNA expression profiles for CRC and adjacent tissues from the TCGA database. Employing R software for data analysis, a volcano plot was conducted to depicte the differential expression of miRNAs in CRC, which indicated that miR-144-3p is markedly overexpressed in CRC (Fig. 1A). Subsequently, the expression levels of miR-144-3p in CRC tissues were examined using TCGA data, revealing that miR-144-3p is significantly overexpressed in malignant tissues (Fig. 1B). In Fig. 1C, the impact of miR-144-3p on the survival of CRC patients was further investigated through survival analysis conducted in the oncomiR database (https://oncomir.org/ReasonOncomiR). Additionally, the analysis of pathological staging data from the oncomiR database demonstrated a robust correlation between miR-144-3p and pathological staging in CRC (Fig. 1D). Moreover, the expression of miR-144-3p in CRC tumor samples was quantified by qRT-PCR, with elevated levels observed in 3 out of 4 samples (Fig. 1E). Furthermore, when comparing the expression levels of miR-144-3p between CRC cells (SW620, HCT116) and HIEC, it was noted that miR-144-3p was considerably overexpressed in CRC cells (Fig. 1F). In conclusion, miR-144-3p is upregulated in CRC and appears to be linked to tumorigenesis.

3.2 MiR-144-3p promotes the proliferation, migration and invasion of CRC cells

Inhibitor and mimics of miR-144-3p were developed and their efficacy was confirmed in SW620 and HCT116 cells through qRT-PCR analysis (Fig. 2A, B). To assess their influence on the oncogenic properties of CRC cells, CCK-8 assays were performed to evaluate cell viability at 0 h, 24 h, 48 h, and 72 h following transfection with miR-144-3p mimics and inhibitor. The findings indicated that the proliferation of SW620 and HCT116 was markedly diminished by the miR-144-3p inhibitor (Fig. 2C, D). The ratio of proliferating cells (EdU-positive) to total cells (DAPI-stained) was examined using EdU assays 48 h post-transfection. The data revealed a significant reduction in cell proliferation in SW620 and HCT116 upon miR-144-3p inhibition, implying a dampened proliferative capacity (Fig. 2E-H), with Fig. 2G and H summarizing the statistical outcomes. Subsequently, the clonogenic potential was assessed 14 days post-transfection using crystal violet staining, which demonstrated a significant attenuation in the growth vigor of CRC cells due

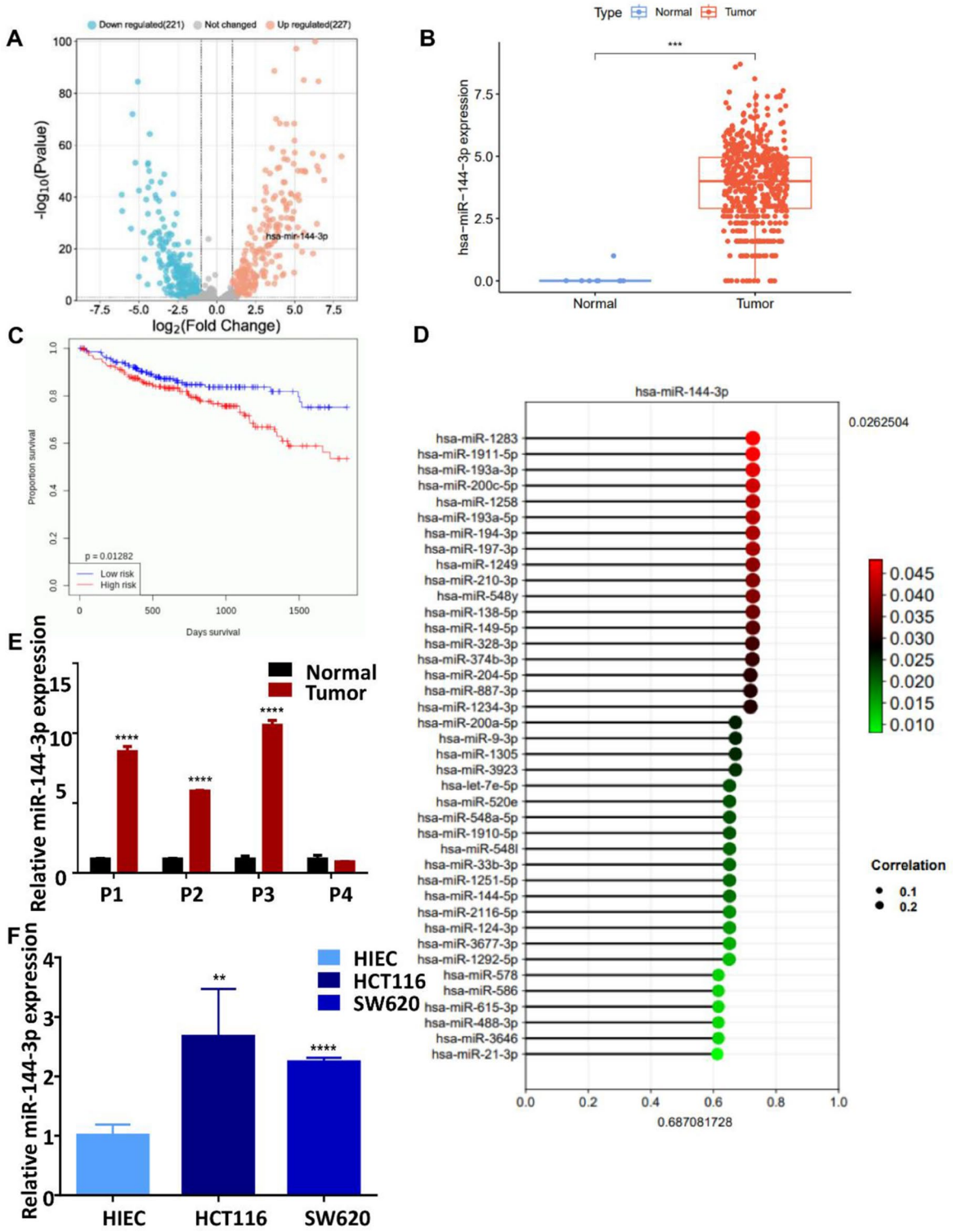

Fig. 1 MiR-144-3p is upregulated in CRC and associated with tumor progression. (**A**) A volcano plot was showed the expression of miR-144-3p in colorectal cancer based on data from the TCGA database. (**B**) A box plot was displayed the expression levels of miR-144-3p in colorectal cancer from the TCGA database. (**C**) The survival curves of colorectal cancer patients with high and low expression of miR-144-3p. (**D**) The dotted line graph indicated the correlation between miR-144-3p and pathological M staging. (**E**) QRT-PCR data showed the expression levels of miR-144-3p in tissue samples from four colorectal cancer patients. (**F**) QRT-PCR analysis indicated the expression levels of miR-144-3p in colorectal cancer cells. (Treatment group vs. control group; $*p<0.05$, $**p<0.01$, $***p<0.001$)

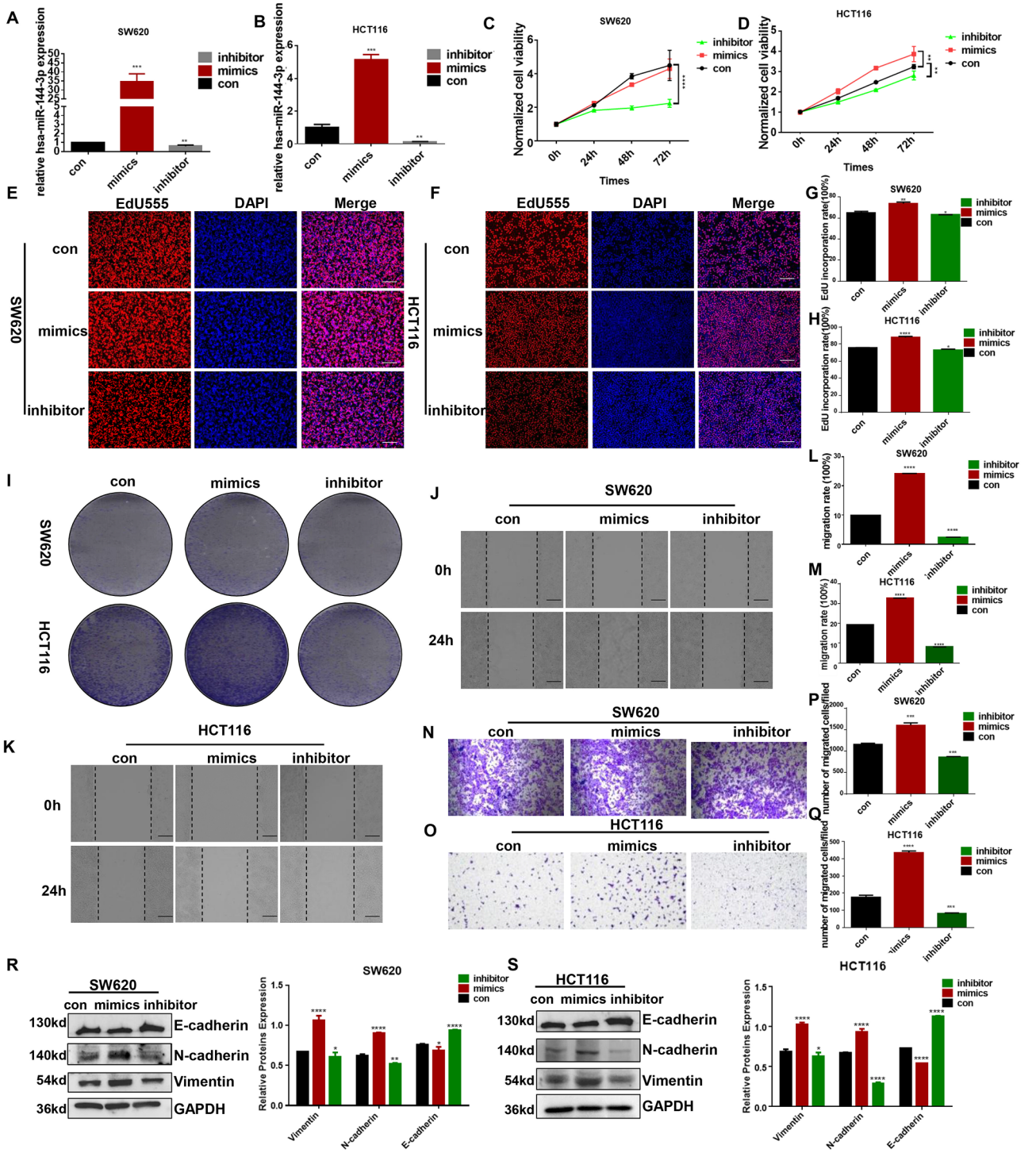

to miR-144-3p inhibition (Fig. 2I). Wound healing assays conducted 48 h post-transfection to evaluate migration over a 24-hour period showed that miR-144-3p inhibition significantly hindered cell motility (Fig. 2J-M), with Fig. 2L and M compiling the final statistical data. Furthermore, the invasive potential of CRC cells was evaluated 48 h post-transfection using Transwell assay, which indicated that inhibiting miR-144-3p expression substantially curtailed cell invasion (Fig. 2N-Q), with Fig. 2P and Q presenting the conclusive statistical findings. Besides, WB analysis of E-cadherin, N-cadherin and Vimentin demonstrated that the miR-144-3p inhibition significantly suppressed the EMT activation pathway in SW620 and HCT116 cells (Fig. 2R, S).

Additionally, following treatment with 5-FU, the levels of miR-144-3p were observed to decrease in SW620 cells

Fig. 2 MiR-144-3p promotes the proliferation, migration and invasion of CRC cells. (**A**) QRT-PCR was used to measure the expression of miR-144-3p in SW620 and HCT116 (**B**) cells by transfected with the constructed miR-144-3p mimics and inhibitor. (**C**) Line charts were used to present the relative cell viability of SW620 and HCT116 (**D**) cells at 0,24,48, and72 hours post-treatment, as determined by the CCK-8 assay. (**E**) EdU experiment was conducted to assess the proliferation of SW620 and HCT116 (**F**) cells after treatment with mimics and inhibitor, visualized under a 10x inverted fluorescence microscope with a 10 μm scale bar. (**G** and **H**) Statistical graphs quantified the results from the EdU experiment. (**I**) A cell colony formation assay was performed on SW620 and HCT116 cells treated with mimics and inhibitor for 14 days. (**J**) Wound-healing assays were conducted to evaluate the proliferation and migration abilities of SW620 and HCT116 (**K**) cells transfected with mimics and inhibitor, imaged under a 10x inverted fluorescence microscope with a 10 μm scale bar. (**L** and **M**) Statistical graphs quantified the results from the wound-healing assays. (**N**) A Transwell invasion assay was performed to assess the invasiveness of SW620 and HCT116 (**O**) cells, visualized under a 10x inverted fluorescence microscope with a 10 μm scale bar. (**P** and **Q**) Statistical graphs quantified the results from the Transwell invasion assay. E-cadherin, N-cadherin, Vimentin was detected by WB assay transfected with mimics and inhibitor in SW620 (**R**) and HCT116 (**S**) cells. (Treatment group vs. control group; $*p<0.05$, $**p<0.01$, $***p<0.001$)

(Fig. S2A). A 5-FU-resistant HCT116 cell line was established through chronic exposure to 5-FU, and its resistance was confirmed by determining the IC50 (Fig. S2B). The miR-144-3p levels in the 5-FU-resistant HCT116 cells were found to be lower compared to those in the non-treated HCT116 cells (Fig. S2C). Utilizing miR-144-3p mimics and inhibitor in HCT116R cells, assays including scratch wound healing, EdU, CCK-8, and colony formation assays demonstrated that elevating miR-144-3p levels suppressed the proliferation of the 5-FU-resistant cells (Fig. S2D-G), suggesting that miR-144-3p plays a role in the resistance of CRC to 5-FU.

In summary, the results suggest that inhibiting miR-144-3p expression suppresses the malignant behavior of CRC, which further stimulates the exploration into the potential mechanisms through which miR-144-3p exerts its effects.

3.3 MiR-144-3p restrains cuproptosis and apoptosis with binding to the 3′-UTR of *PUMA* mRNA

To explore the regulatory mechanism of miR-144-3p, we initially investigated its impact on the expression of proteins associated with cell death (Fig. S3A, B). Our findings revealed that the aggregation of the cuproptosis-related proteins DLAT and DLST was markedly enhanced while LIAS was significantly reduced upon treatment with the miR-144-3p inhibitor, whereas the opposite effect was noted with miR-144-3p mimics (Fig. 3A, B), suggesting a possible link between miR-144-3p and cuproptosis. Utilizing TargetScan7.2 prediction, we discovered that DLAT/DLST/LIAS mRNAs are not a target of miR-144-3p (Supplementary Material 4). Consequently, we focused on genes within the mitochondria, the primary site of cuproptosis. We intersected genes with reduced expression in CRC from the GEO dataset (GSE44076, GSE41258, GSE113513, GSE103512, GSE44861, GSE39582, GSE20916) with mitochondrial-related gene (Supplementary Material 5) sets from Human MitoCarta 3.0 (Human MitoCarta3.0) and target genes of miR-144-3p (Supplementary Material 6), identifying PUMA as the sole overlapping gene (Fig. 3C). The binding site of miR-144-3p to the 3′-UTR of *PUMA* mRNA was further predicted (Fig. 3D). Based on this binding site, mutant (MUT-PUMA) and wild-type (WT-PUMA) constructs were generated. Following co-transfection of these constructs with miR-144-3p mimics in CRC cells, dual-luciferase assays confirmed that PUMA is bound by miR-144-3p at the predicted site, p-value < 0.001 (Fig. 3E). Additionally, RIP experiments validated that PUMA 3′-UTR binding sequences were more enriched in the anti-AgO_2 group compared to the anti-IgG group, p-value = 0.0424 (Fig. 3F). Moreover, qRT-PCR and Western blot analyses demonstrated that both mRNA and protein levels of PUMA were downregulated in the miR-144-3p mimic treatment group and upregulated in the inhibitor treatment group (Fig. 3G-J), indicating that miR-144-3p binding to the 3′-UTR of *PUMA* mRNA suppresses PUMA expression.

PUMA is a pro-apoptotic protein critical for cell death regulation. WB experiments showed that treatment with miR-144-3p mimics significantly increased the expression of apoptosis-related markers Caspase3 and BCL-2, while the levels of Cleaved Caspase3 and BAX exhibited a decreasing trend. Conversely, treatment with the miR-144-3p inhibitor yielded divergent results (Fig. 3K, L). Furthermore, IF experiments confirmed that treatment of HCT116 cells with the miR-144-3p inhibitor led to a noticeable translocation of BAX protein to the mitochondria (Fig. 3M). Subsequently, apoptosis-relative flow cytometry analysis revealed that cell apoptosis was significantly reduced in the miR-144-3p mimic group and markedly increased in the miR-144-3p inhibitor group compared to the control group (Fig. 3N, O). Lastly, measurement of intracellular ROS levels showed that inhibition of miR-144-3p expression resulted in a significant increase in intracellular ROS levels (Fig. 3P, Q), further substantiating the regulatory role of miR-144-3p in apoptosis.

3.4 PUMA induces cuproptosis by accelerating DLAT and DLST oligomerization

The present study further investigated the relationship between PUMA, the molecule regulated by miR-144-3p, and cuproptosis. With increasing concentrations of Elesclomol

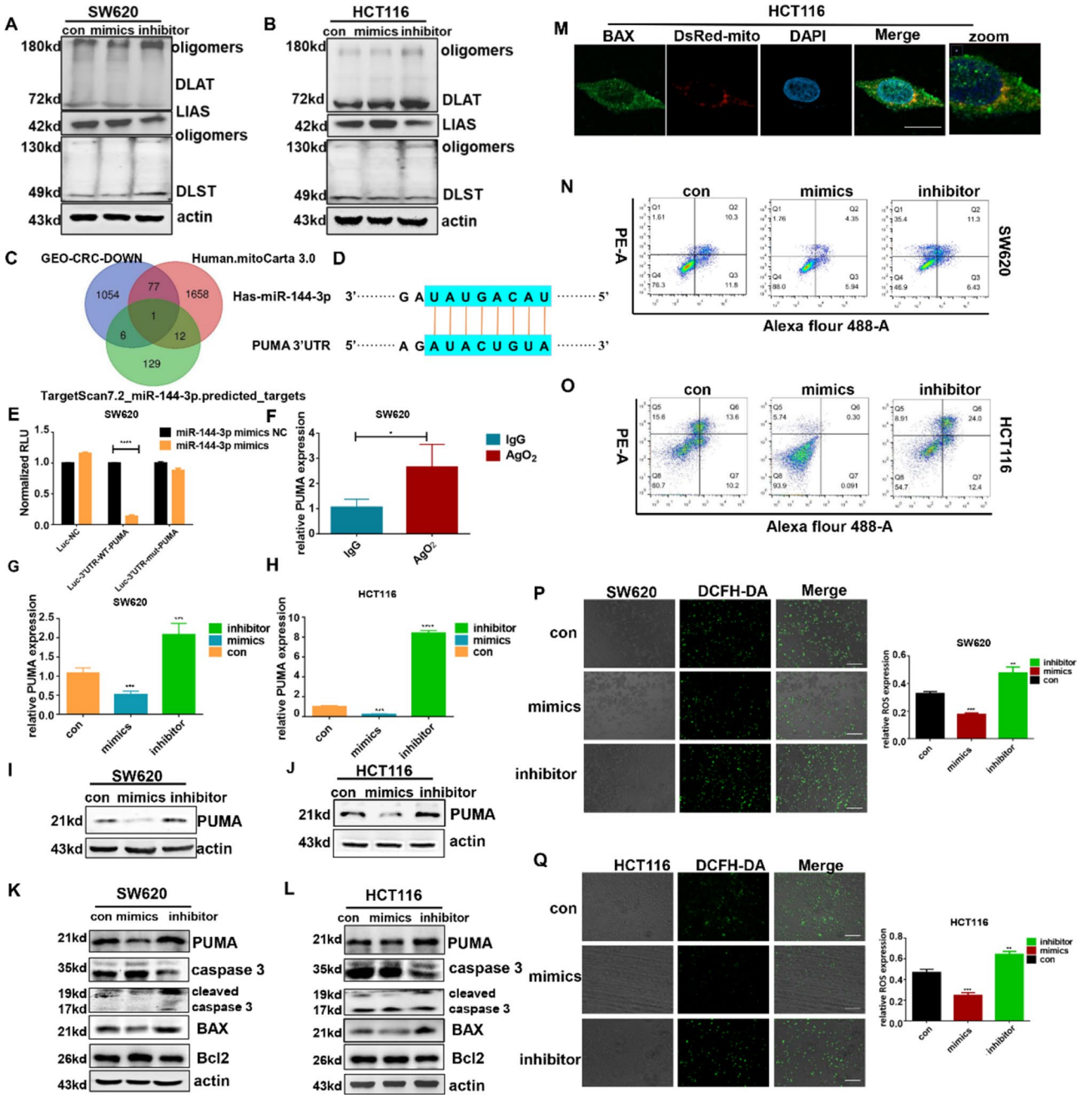

Fig. 3 MiR-144-3p restrains cuproptosis and apoptosis with binding to the 3′-UTR of *PUMA* mRNA. (**A**) The cuproptosis-related proteins (DLAT, DLST and LIAS) were detected in SW620 and HCT116 (**B**) cells transfected with mimics and inhibitor. (**C**) Venn diagram was drawn from CRC datasets in the GEO database, the Human mitoCarta dataset, and target data for miR-144-3p from TargetScan. (**D**) Schematic diagram was used to illustrate the binding sequence between miR-144-3p and PUMA. (**E**) The dual-luciferase assay was displayed the connection between miR-144-3p and PUMA co-transfected with mimics, WT-PUMA and MUT-PUMA. (**F**) RIP assay was used to measure the expression of PUMA fragments between anti-AgO_2 group and anti-IgG group. (**G** and **H**) QRT-PCR and (**I** and **J**) WB experiments were detected to the mRNA and protein level of PUMA in SW620 and HCT116 after treatment with mimics and inhibitor. (**G**) The apoptosis-related proteins were detected in SW620 and HCT116 (**L**) cells transfected with mimics and inhibitor. (**M**) The location of Bax was imaged by confocal microscopy in HCT116 transfected miR-144-3p inhibitor. (**N**) Flow Cytometry was used to detect SW620 and HCT116(**O**) cells apoptosis after treatment with mimics and inhibitor. (**P**) ROS assay was conducted to evaluate the ROS level of SW620 and HCT116 (**Q**) cells transfected with mimics and inhibitors, imaged under a 10x inverted fluorescence microscope with a 10μm scale bar. (Treatment group vs. control group; $*p<0.05$, $**p<0.01$, $***p<0.001$)

(Fig. S4A, B) and Disulfiram (Fig. S4C, D) in combination with the same concentrations of $CuCl_2$, the expression of PUMA progressively elevated in SW620 and HCT116 cells. Initially, OE-PUMA, shPUMA1, and shPUMA2 were transfected into SW620 and HCT116 cells, revealing a positive correlation between DLAT/DLST oligomerization and PUMA levels, while a negative correlation between LIAS and PUMA expression (Fig. 4A, B). Subsequently, HCT116 and HCT116 $^{PUMA-/-}$ cells were exposed to various concentrations of Elesclomol with the same concentrations of $CuCl_2$ for 24 h, and the results demonstrated that the effects of Cu^+ on the cells were mitigated by PUMA knockout (Fig. 4C), indicating that PUMA enhances cuproptosis. Furthermore, OE-PUMA of HCT116 cells showed increased DLAT oligomerization, as evidenced by IF experiments (Fig. 4D, Fig. S4E). Additionally, co-treatment with OE-PUMA, shPUMA1, or shPUMA2 along with miR-144-3p mimics or inhibitor revealed that decreased PUMA levels correlated with reduced DLAT/DLST oligomerization and higher LIAS expression (Fig. 4E, F). Conversely, elevated PUMA levels promoted DLAT/DLST oligomerization and suppressed LIAS expression (Fig. 4G, H).

To delve deeper into the PUMA-cuproptosis nexus, small-molecule compounds that elevate PUMA expression, such as Triacetylresveratrol (TRES), 5-FU, and OSI-027, were utilized. Treatment with escalating concentrations of TRES (Fig. 4I, J), 5-FU (Fig. 4K, L), and OSI-027 (Fig. 4M, N) for 48 h in SW620 and HCT116 cells led to enhanced DLAT/DLST oligomerization and suppressed LIAS expression. Studies have established that GSH can suppress cuproptosis [33]. Accordingly, GSH levels were assessed under identical treatment conditions with TRES, 5-FU, and OSI-027, and it was demonstrated that as drug concentrations escalated, GSH levels progressively declined (Fig. 4O-T). These findings suggest that PUMA induces cuproptosis by promoting DLAT/DLST oligomerization.

While PUMA is established as a p53-dependent effector of DNA damage-induced apoptosis [34], its role in cuproptosis-associated DNA damage remains unclear. To investigate this, we treated SW620 cells with OE-PUMA, shPUMA1, shPUMA2, Elesclomol-$CuCl_2$ (1μM each). Comet assays revealed significant DNA damage in OE-PUMA and Elesclomol-$CuCl_2$ groups (Fig. S5A), evidenced by increased % tail DNA (Fig. S5B) and Olive Tail Moment (Fig. S5C). Parallel experiments in HCT116 cells confirmed that cuproptosis induction consistently accompanies DNA damage (Fig.S5D-F). These findings suggest DNA damage may be a downstream consequence of cuproptosis.

3.5 PUMA directly binds to FDX1 at the R155 site thus inducing cuproptosis

To further investigate into the role of PUMA in cuproptosis, we concentrated on FDX1, which facilitates the oligomerization of lipoylated DLAT/DLST, thereby initiating cuproptosis [33]. Consequently, we explored the potential interaction between PUMA and FDX1. Molecular docking suggested that PUMA directly interacts with FDX1, with a binding energy of -22 kcal/mol, mediated by hydrogen bonds and salt bridges (Fig. 5A), and further details are presented in Fig. S6A and Table S5. Subsequently, IF experiment in HCT116 cells demonstrated co-localization of FDX1 with TOM20 (Fig. 5B), indicating that FDX1 resides in the outer mitochondrial membrane. The mCherry-FDX1 construct was generated and confirmed (Fig. S6B), and it was observed to co-localize with mito-tracker Green in SW620 cells (Fig. S6C). Additionally, IF assays and live-cell imaging revealed co-localization of FDX1 with PUMA (Fig. 5C and D). Reciprocal Co-IP with anti-PUMA and anti-FDX1 antibodies demonstrated a direct PUMA-FDX1 interaction (Fig. 5E-H). Following this, to pinpoint the binding site of PUMA on FDX1, plasmids encoding distinct PUMA protein domains were constructed (Fig. S6D). After transfection with these plasmids and MYC-FDX1, Co-IP assays were conducted, revealing that the absence of a specific domain impacted the binding of PUMA and FDX1, suggesting that PUMA bound to FDX1 at the R155 site (Fig. 5I). Furthermore, in SW620 and HCT116 cells co-transfection of OE-PUMA and siFDX1, the OE-PUMA induced increase in lipoylated DLAT/DLST oligomerization was attenuated by siFDX1. This finding indicates that the effect of PUMA on the oligomerization of lipoylated DLAT/DLST during cuproptosis is dependent on the functional role of FDX1 (Fig. 5J, K). Moreover, these results further substantiate that the regulation of PUMA in the induction of cuproptosis relies on its interaction with FDX1. In summary, the collective findings from these various experiments demonstrate that PUMA binds to FDX1 at the R155 site, thereby enhancing FDX1's role in the oligomerization of lipoylated DLAT/DLST and the initiation of cuproptosis.

3.6 PUMA participates the ubiquitination of FDX1 at the K182 site which leads to the degradation of FDX1 during cuproptosis

At the terminal stage of cuproptosis, the loss of iron-sulfur cluster proteins occurs, leading to cell death. Among these proteins, FDX1, which is a member of the iron-sulfur cluster family, also diminishes during cuproptosis [33]. To elucidate the reason behind the decrease in FDX1 levels during cuproptosis, we examined the ubiquitination levels of

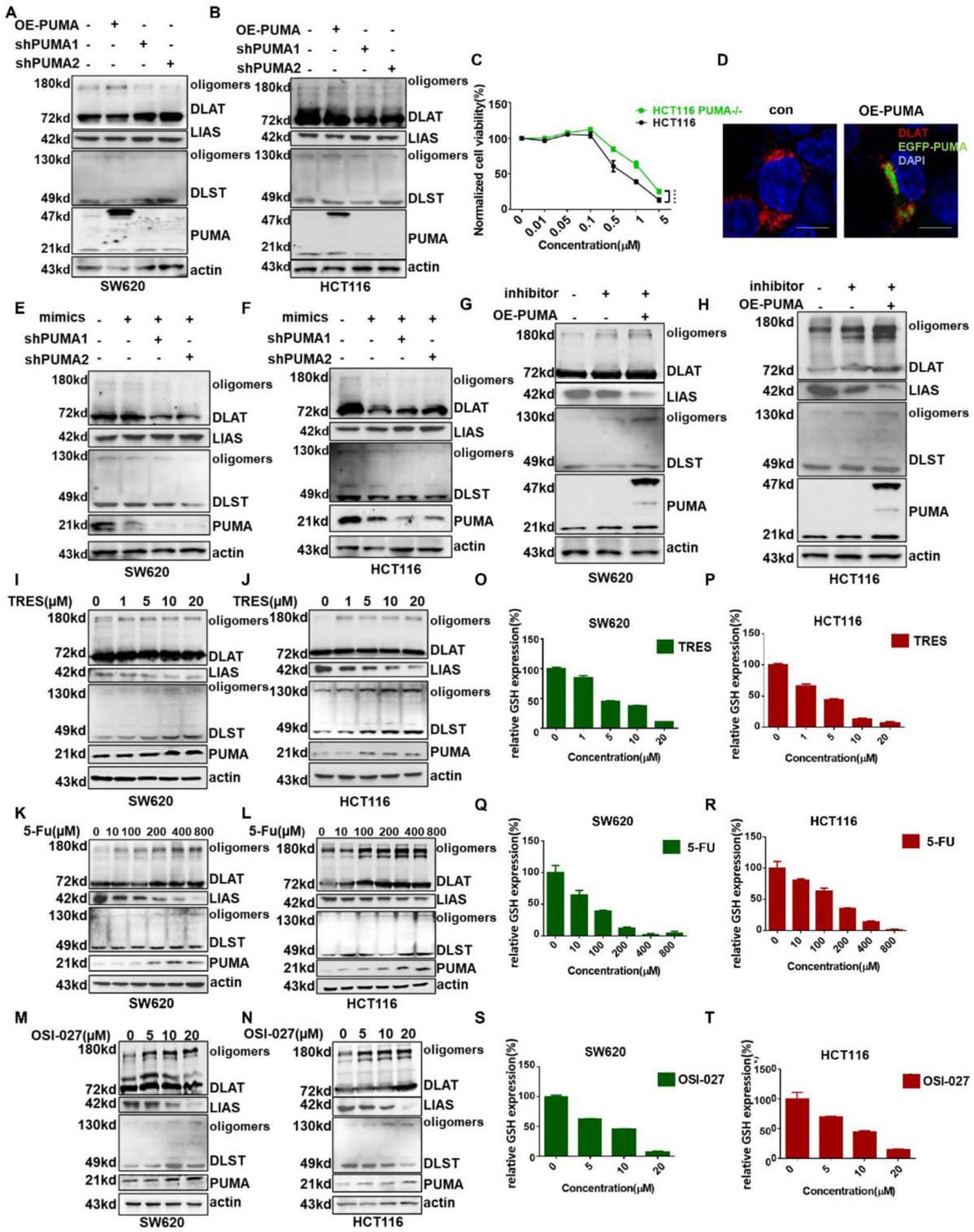

FDX1, a process that is prevalent in protein interaction [35]. Co-IP experiments revealed that the levels of HA-ubiquitin (HA-UB) were elevated in the cuproptosis group compared to the con, indicating that FDX1 undergoes ubiquitination-mediated degradation (Fig. 6A). To further investigate the ubiquitination-mediated degradation of FDX1 during cuproptosis, we focused on PUMA, which has been recently identified as a critical regulator in ubiquitination processes [36]. OE-PUMA, shPUMA1, and shPUMA2 plasmids were utilized to modulate PUMA expression during cuproptosis. The results demonstrated that the ubiquitination level of FDX1, which was elevated during cuproptosis, was further

Fig. 4 PUMA induces cuproptosis by accelerating DLAT oligomerization. (**A**) The expression level of PUMA, LIAS and DLAT/DLST oligomerization were detected in SW620 and HCT116(**B**) cells transfected with OE-PUMA, shPUMA1,or shPUMA2. (**C**) Cell viability of HCT116 and HCT116$^{PUMA-/-}$ was analyzed by CCK-8 assay in different concentration (0μM, 0.01μM, 0.05μM, 0.1μM, 0.5μM, 1μM, and 5μM) of Elecslomol with same concentration of $CuCl_2$ after 24 h. (**D**) The oligomerization of DLAT was imaged by confocal microscopy in SW620 transfected with OE-PUMA. (**E**) The expression levels of DLAT/DLST oligomerization, LIAS and PUMA were evaluated in SW620 and HCT116 (**F**) cells transfected with miR-144-3p mimics, shPUMA1, or shPUMA2. (**G**) DLAT/DLST oligomerization, LIAS and PUMA were shown in SW620 and HCT116 (**H**) cells by WB transfected with miR-144-3p inhibitor or OE-PUMA. (**I**) WB tested the oligomerization of DLAT/DLST, LIAS, PUMA in SW620 and HCT116 (**J**) cells with different concentration (0μM, 1μM, 5μM, 10μM, and 20μM) of TRES. (**K**) The oligomerization of DLAT and PUMA were shown in SW620 and HCT116 (**L**) cells treated different concentration (0μM, 10μM, 100μM, 200μM, 400μM and 800μM) of 5-FU. (**M**) The oligomerization of DLAT/DLST, LIAS and PUMA levels were assessed in SW620 and HCT116 (**N**) cells treated with OSI-027 at varying concentrations (0μM, 5μM, 10μM, and 20μM). (**O**-**T**) The level of GSH was measured in SW620 and HCT116 cells treated with different concentrations of TRES, 5-FU and OSI-027. (Treatment group vs. control group; *$p<0.05$, **$p<0.01$, ***$p<0.001$)

increased upon PUMA overexpression. Conversely, this effect was significantly reduced when PUMA expression was knocked down (Fig. 6B). These findings suggest that PUMA plays a regulatory role in modulating the ubiquitination of FDX1 during cuproptosis.

Additionally, a negative correlation between FDX1 and PUMA expression was observed. This inverse association was further validated using GEPIA (http://gepia.cancer-pku.cn/Reason) (Fig. 6C). When miR-144-3p mimics and inhibitor were transfected into SW620 and HCT116 cells, a decrease in FDX1 was notably observed with the inhibitor (Fig. S7A, B). Subsequently, when miR-144-3p mimics, shPUMA1, and shPUMA2 were transfected into SW620 and HCT116 cells, an increase in FDX1 expression was noted with the suppression of PUMA expression (Fig. 6D, E). Moreover, co-transfection of miR-144-3p inhibitor and OE-PUMA into SW620 and HCT116 cells resulted in an increase in PUMA expression and a corresponding decrease in FDX1 expression (Fig. 6F, G). Additionally, treatment of SW620 and HCT116 cells with TRES, 5-FU, and OSI-027 also led to a significant decrease in FDX1 expression (Fig. S7C-H). To further investigate the ubiquitination sites of FDX1, four potential ubiquitination sites (K82, K84, K158, and K182) were predicted using the IUUCD2.0 database (http://iuucd.biocuckoo.org/). To ascertain the functional site, mutations were introduced at these ubiquitination sites individually. Consequently, MYC-FDX1-K82R, MYC-FDX1-K84R, MYC-FDX1-K158R, and MYC-FDX1-K182R plasmids were constructed as depicted in Fig. 6H. After successful confirmation of the plasmid sequences, the effects of these plasmids were validated at the protein level (Fig. S7I). These plasmids and MYC-FDX1-WT were co-transfected with HA-UB into 293T cells, and Co-IP experiments after 48 h indicated that the ubiquitination level of FDX1 was significantly reduced when the K182 site was mutated (Fig. 6I), suggesting that FDX1 is ubiquitinated at the K182 site. Furthermore, ubiquitin ligases predicted to interact with PUMA and FDX1 were identified, providing additional evidence that PUMA is involved in the ubiquitination process of FDX1(Fig. S7J).

In conclusion, during cuproptosis, the ubiquitination level of FDX1 is elevated at the K182 residue, resulting in the degradation of FDX1. Furthermore, PUMA plays a critical role in this process.

3.7 Activating PUMA by inhibiting miR-144-3p reduces CRC progression in vivo

To further probe the impact of PUMA modulation by miR-144-3p inhibition on tumorigenesis in vivo, two constructs were generated: OE-miR-144-3p and sh-miR-144-3p. Their expression was confirmed using qRT-PCR (Fig. 7A, B). CCK-8 assay revealed that cells with sh-miR-144-3p exhibited suppressed CRC cell proliferation, whereas those with OE-miR-144-3p did not (Fig. 7C, D). Following this, the regulatory effect of miR-144-3p on PUMA was validated by qRT-PCR (Fig. 7E, F) and Western blot analysis (Fig. 7G, H). Subsequently, HCT116$^{OE-miR-144-3p}$ and HCT116$^{sh-miR-144-3p}$ cell lines were developed. Tumor xenograft experiments in nude mice were initiated using these cell lines. The body weight (Fig. 7I) and tumor growth (Fig. 7J) of the mice were monitored over a 14-day period. Upon experiment termination, the subcutaneous tumors were resected, and their dimensions were documented (Fig. 7K). In the miR-144-3p-overexpressing group, accelerated tumor growth and larger tumor sizes were observed, while the group with suppressed miR-144-3p displayed significantly smaller tumors with decelerated growth rates. Additional qRT-PCR data indicated that in the OE-miR-144-3p group, PUMA mRNA levels were markedly reduced, whereas in the sh-miR-144-3p group, *PUMA* mRNA levels were considerably elevated (Fig. 7L). Moreover, Western blot results demonstrated that in the sh-miR-144-3p group, PUMA protein levels were upregulated compared to the control, FDX1 expression was diminished, and DLAT oligomerization was enhanced (Fig. 7M). Furthermore, immunohistochemistry analysis (Fig. 7N) showed that in the sh-miR-144-3p group, there was a decrease in the cell proliferation marker Ki67 expression, accompanied by increased PUMA and FDX1 expressions. Collectively, these results underscore the pivotal regulatory role of miR-144-3p on PUMA and FDX1 in tumorigenesis (see Fig. 8).

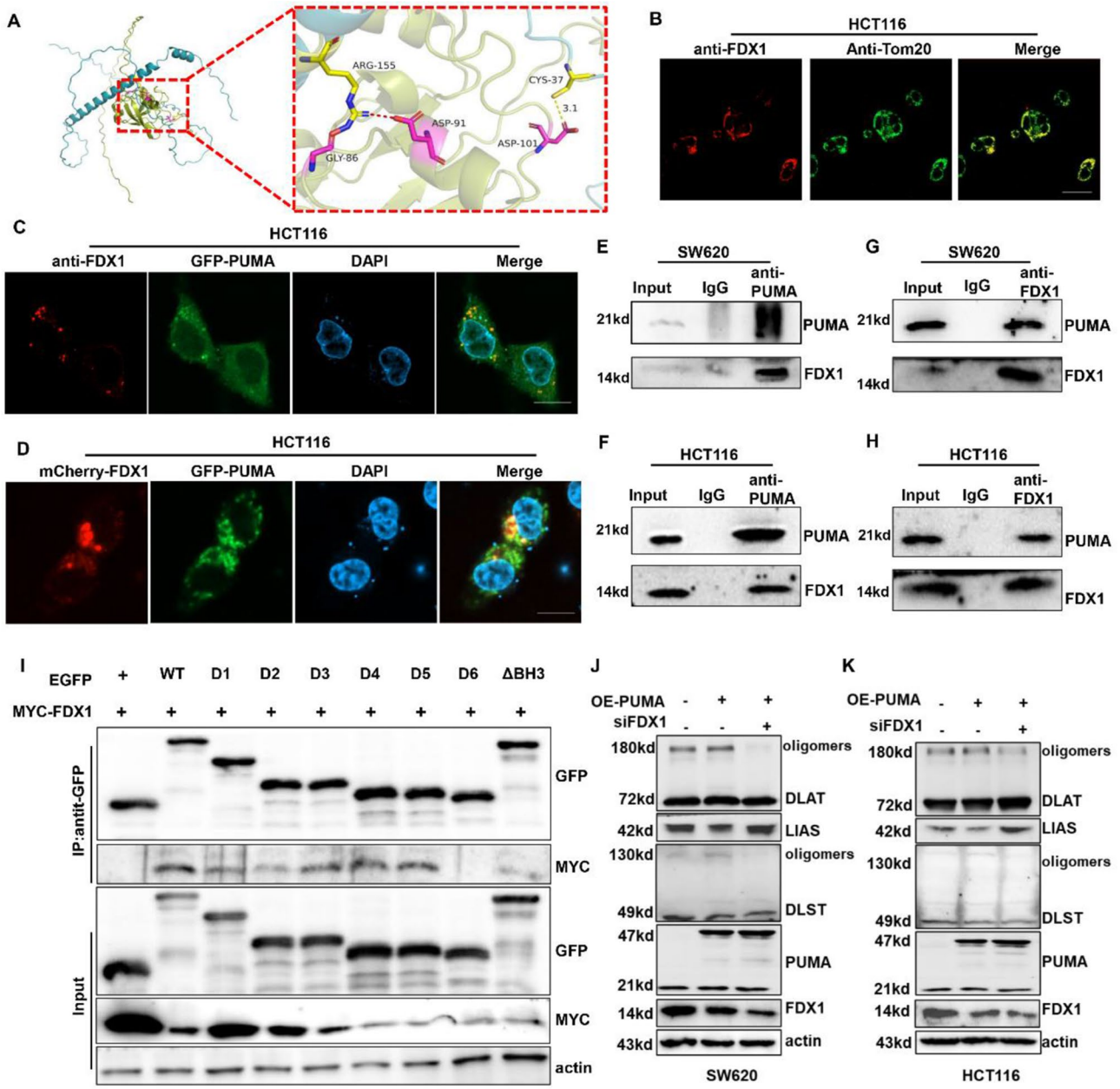

Fig. 5 PUMA directly binds to FDX1 at the R155 site thus inducing cuproptosis. (**A**) Molecular docking was used to detect the binding between FDX1 and PUMA. (**B**) The co-localization of FDX1 and TOM20 was imaged by IF. (**C**) The co-localization of FDX1 and GFP-PUMA was observed by IF. (**D**) The localization of mCherry-FDX1 and GFP-PUMA was shown using live-cell imaging. (**E**) Co-IP experiment revealed that FDX1 interacted with PUMA in SW620 and HCT116 (**F**) cells. (**G**) Co-IP experiment revealed FDX1-PUMA interaction in SW620 and HCT116 (**H**) cells. (**I**) Co-IP experiment revealed that MYC-FDX1 interacted with GFP-PUMA in HCT116. (**J**) The expression levels of DLAT/DLST oligomerization and LIAS were detected in SW620 and HCT116 (**K**) cells that were transfected with OE-PUMA and siFDX1

4 Discussion

Studies indicated that cuproptosis plays an important role in various physiological processes, including cell development and immune response [37]. Additionally, cuproptosis is linked to multiple diseases, particularly gastrointestinal cancers and neurodegenerative diseases [38]. In the present study, PUMA was found to induce cuproptosis by binding to FDX1 and enhancing its function in CRC. Moreover, the ubiquitination of FDX1 was found to increase at the K182 site, which led to the degradation of FDX1 during cuproptosis.

PUMA is known as a key pro-apoptotic protein that plays an important role through several mechanisms: PUMA is

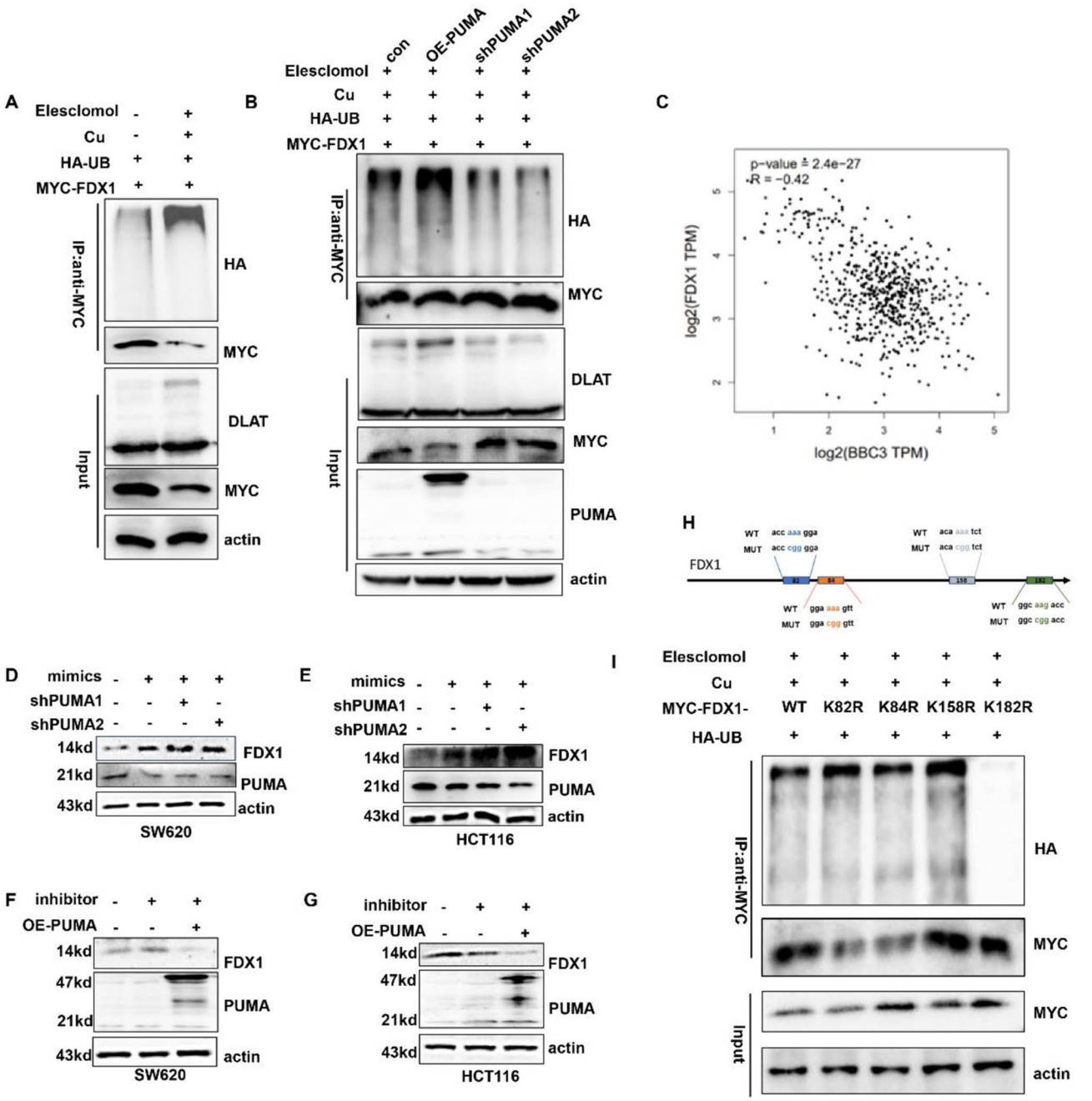

Fig. 6 PUMA participates the ubiquitination of FDX1 at the K182 site which leads to the degradation of FDX1 during cuproptosis. (**A**) The relative ubiquitination level of FDX1 was detected using a Co-IP experiment in 293T cell treated with 1μM Elesclomol and 1μM $CuCl_2$. (**B**) The relative ubiquitination level of FDX1 was shown by Co-IP in 293T cells treated with 1μM Elesclomol and 1μM $CuCl_2$ and transfected with OE-PUMA, shPUMA1 and shPUMA2. (**C**) The correlation between FDX1 and BBC3 was shown in scatter plot through the GEPIA. (**D**) The expression level of FDX1 and PUMA were evaluated in SW620 and HCT116(**E**) cells transfected mimics, shPUMA1, shPUMA2. (**F**) FDX1 and PUMA levels were shown in SW620 and HCT116(**G**) cells by WB experiment with transfected with inhibitor and OE-PUMA. (**H**) The construction of MYC-FDX1-K82R, MYC-FDX1-K84R, MYC-FDX1-K158R and MYC-FDX1-K182R plasmids with site-directed mutations in FDX1 was shown in a schematic diagram. (**I**) The ubiquitination sites of FDX1 were identified through a Co-IP treated with 1μM Elesclomol and 1μM $CuCl_2$

a target gene of p53, capable of inducing apoptosis, especially when cells are under stress or damage [39]. Additionally, PUMA is crucial in regulating the cell cycle and can inhibit cell proliferation [40]. In cases of DNA damage, the expression of PUMA is upregulated, aiding cells in eliminating potential cancerous cells through apoptosis [41]. Due to its pro-apoptotic characteristics, PUMA is considered to prevent tumor formation importantly. Furthermore, PUMA

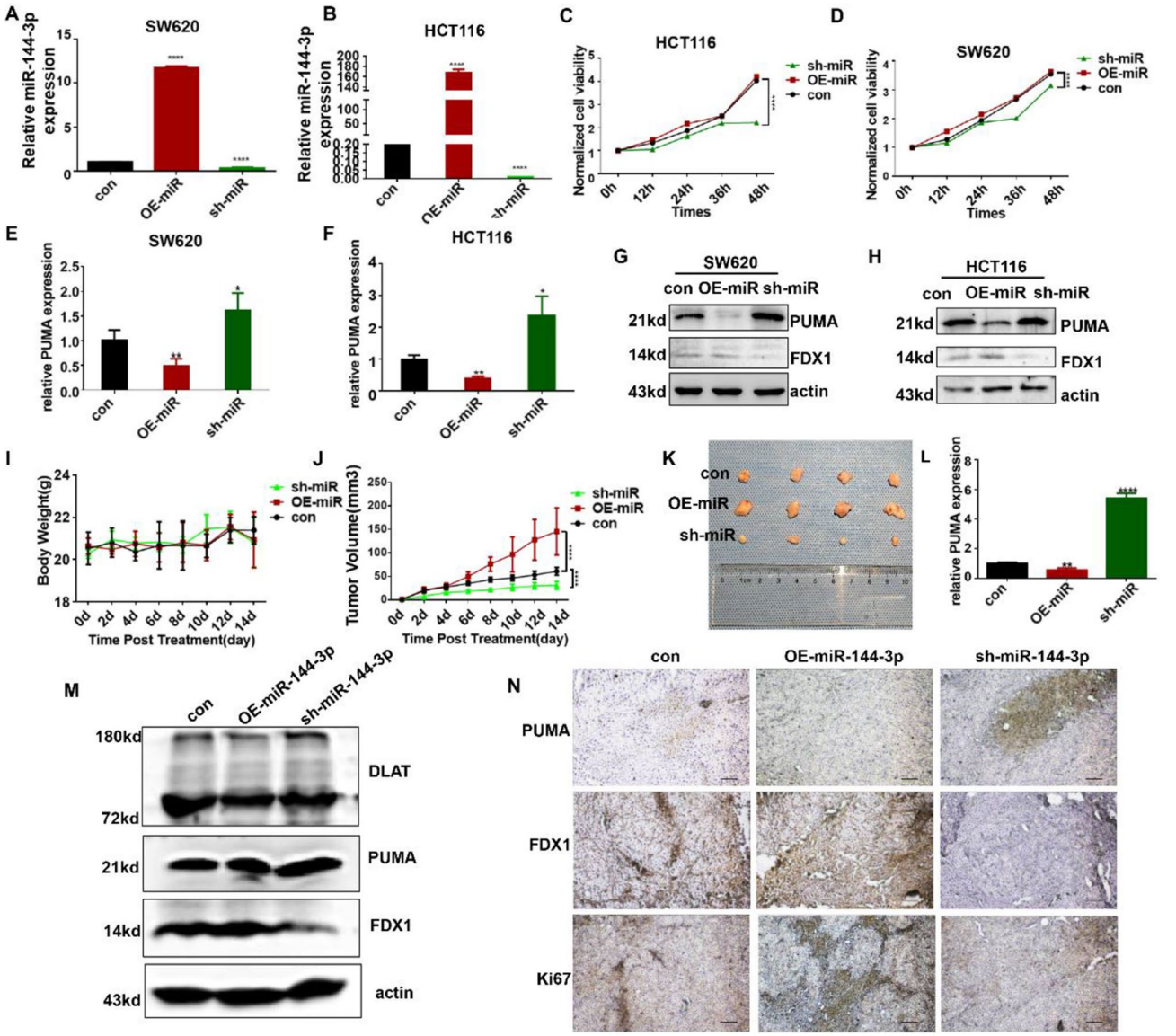

Fig. 7 Activating PUMA by inhibiting miR-144-3p reduces CRC progression in vivo. (**A**) The OE-miR-144-3p and sh-144-3p plasmids were constructed, and the expression level of miR-144-3p in SW620 and HCT116 (**B**) was measured using qRT-PCR. (**C**) The expression level of PUMA in SW620 and HCT116 (**D**) cells treated with OE-miR-144-3p and sh-miR-144-3p for 48 h was measured using qRT-PCR. (**E**) After cells were treated with OE-miR-144-3p and sh-miR-144-3p for 24 h, they were plated, and CCK-8 assays of SW620 and HCT116 (**F**) were measured at 0 h, 12 h, 24 h, and 48 h, with the results plotted. (**G**) After cells were treated with OE-miR-144-3p and sh-miR-144-3p for 48 h, the protein levels of PUMA and FDX1 in SW620 and HCT116 (**H**) were assessed. (**I**) Monitor tumor growth changes in nude mice bearing different groups of tumors over a period of 14 days. (**J**) Weight changes in nude mice bearing tumors over a 14-day period for different groups. (**K**) After 14 days, the mice were euthanized and images of the actual tumor sizes were taken. (**L**) The relative level of PUMA mRNA in tumors from different groups was measured using qRT-PCR. (**M**) The protein expression levels of DLAT, PUMA, and FDX1 in tumors from different groups were measured in WB experiment. (**N**) The expression levels of PUMA, FDX1, and Ki67 in tumors from different groups was assessed using immunohistochemistry

is also related to the process of autophagy, potentially regulating the balance between cell survival and death [42]. In this study, we found that apart from inducing apoptosis, PUMA played a new role in inducing cuproptosis, and PUMA knockout CRC cells exhibited sensitively to reduce cuproptosis (Fig. 4C). Moreover, when cells were treated with OE-PUMA, DLAT/DLST showed oligomerization (Fig. 3D), and the same phenomenon was also observed when treating cells with plasmids and various small molecule drugs which could activating PUMA, such as 5-FU, OSI-027, TRES (Fig. 4I-N). GSH levels significantly decreased with increasing drug concentrations (Fig. 4O-T). Additionally, comet assays also demonstrated cuproptosis induction consistently accompanies DNA damage (Fig. S5).

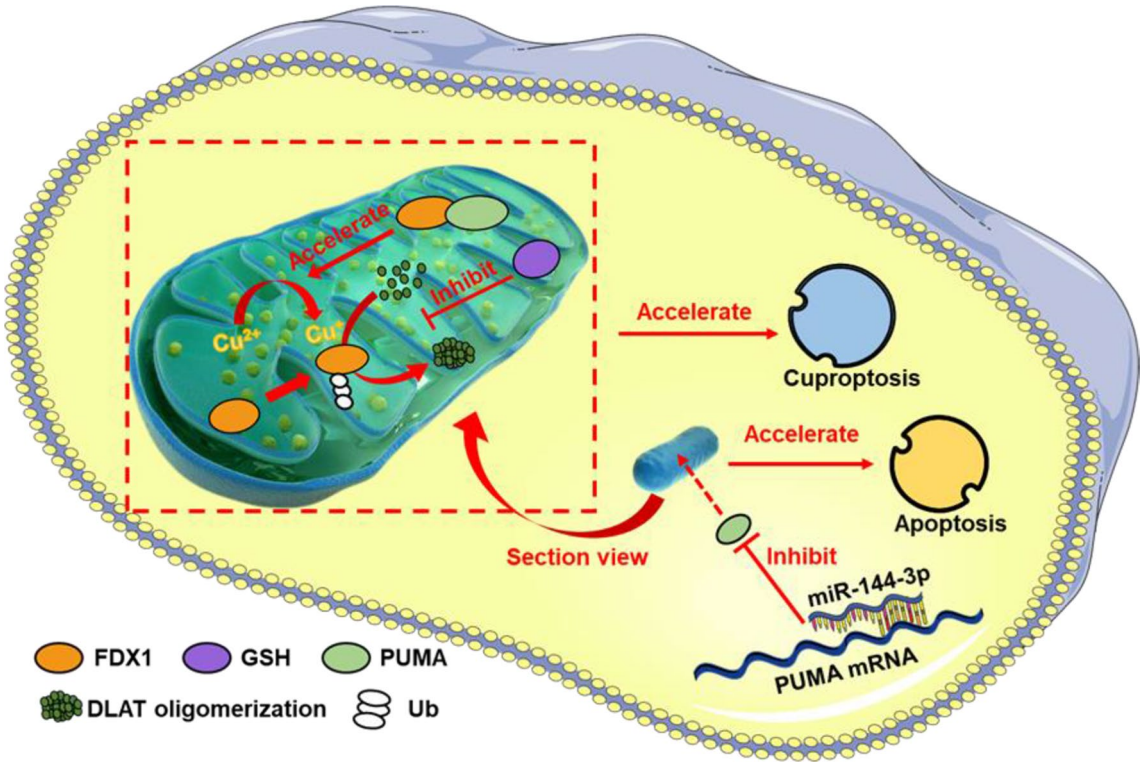

Fig. 8 The mechanism diagram of this study

Expression of PUMA is regulated by various factors, including transcription factors and non-coding RNAs such as miRNAs. For example, previous work from our team has shown that the transcription factor FOXO3a could promote apoptosis by regulating PUMA [25]. Additionally, miR-221/miR-222 alleviate myocardial ischemia-reperfusion injury exacerbated by regulating PUMA [43]. In this study, we found that a highly expressed miR-144-3p is a direct target of *PUMA* mRNA in CRC (Fig. 3C). And their binding sites of 3′-UTR were also identified for the first time (Fig. 3D-F). When miR-144-3p was increased by mimics, PUMA's mRNA and protein diminished, whereas inhibitor increased them (Fig. 3G-J). MicroRNA is recognized as a key mediator in regulating various biological processes such as DNA repair [44], cellular signal transduction [45], metabolism [46], and cell death [47]. The expression of miRNAs has become a research hotspot as diagnostic and prognostic biomarkers for cancer. MiR-144-3p is widely present in various cells and tissues [48]. In our study, we found that miR-144-3p is upregulated in CRC through TCGA (Fig. 1A, B) and is closely associated with pathological M staging (Fig. 1D). Inhibiting the expression of miR-144-3p in CRC cells significantly suppressed the proliferation, migration, and invasion of CRC (Figs. 2A-N and 7N). In addition, miR-144-3p promoted apoptosis (Fig. 4K-G) and cuptoprosis (Figs. 3A and B and E-H) though regulating PUMA.

FDX1 is an important iron-sulfur protein that is closely related to cuproptosis. The regulation of FDX1 expression affects cellular sensitivity to copper, making it a potential target for cancer therapy [49]. The expression of FDX1 is regulated by various factors, including transcription factors and non-coding RNAs (such as miRNAs). For example, Sun et al. found that FDX1 can affect its stability through m6A modification of mRNA, thereby regulating cuproptosis [50]. In our study, we discovered the binding of PUMA and FDX1 through molecular docking, Co-IP experiments and confocal imaging (Fig. 5A-H). meanwhile, the binding site of PUMA and FDX1 was identified (Fig. 5I, J). The view that cuproptosis was connected with the depletion of FDX1 was proved in recent research [33] and our study (Fig. S7A-H). Autophagy and ubiquitin-proteasome system are the most two pathways of protein degradation [51, 52]. It was found that ubiquitination-mediated degradation led to FDX1 depletion in cuproptosis (Fig. 6A). Furthermore, with the change in PUMA expression levels, the oligomerization of DLAT/DLST was changed and the ubiquitination level of FDX1 is consequently affected (Fig. 6B). We constructed plasmids with FDX1 ubiquitination site mutations, MYC-FDX1-K82R, MYC -FDX1-K84R, MYC -FDX1-K158R, and MYC -FDX1-K182R, and through Co-IP experiments, we found that FDX1 ubiquitination disappears when the K182 site is mutated (Fig. 6J). However, the occurrence of ubiquitination requires the involvement of ubiquitin ligases

[53]. Therefore, in the future, we will continue identifying the ubiquitin ligase that mediates FDX1.

Since cuproptosis discovery, it has sparked extensive research. For example, copper-based nanoparticles responsive to near-infrared light have been used for tumor treatment [54], copper-loaded hydrogels and copper nanoparticles activate the immune system for cancer therapy [55, 56]. While cuproptosis has emerged as significant cell death mechanism linked cancer and neurodegeneration, the upstream regulatory networks, particularly involving non-coding RNAs and key cuproptosis executor like FDX1, remain less explored. Current research has primarily focused on the core mechanism involving copper-dependent mitochondrial lipoylation and DLAT oligomerization initiated by FDX1, the identification of copper ionophores inducing cuproptosis, or the metabolic dependencies influencing cellular copper sensitivity [57]. Our study provides distinct insights in several key aspects. We identify a novel and specific miRNA, miR-144-3p, as a direct negative regulator of PUMA, and an innovative, non-apoptotic function of PUMA. We demonstrate that PUMA directly binds to and enhance the function of FDX1, acting as a positive regulator of cuproptosis. Although FDX1 depletion is recognized as a hallmark of cuproptosis, the precise molecular mechanism governing its degradatiom was unclear, we provide direct evidence that FDX1 undergoes ubiquitination specifically at K182 residue. Our findings using PUMA-activating small molecules (5-FU, TRES, OSI-027) to induce DLAT/DLST oligomerization and cuproptosis highlight PUMA as a druggable target distinct from copper modulation.

In summary, it is indicated that the miR-144-3p/PUMA axis induces cells towards cuproptosis by binding to FDX1 and promoting the oligomerization of DLAT/DLST. Additionally, apoptosis can be modulated through the mitochondrial pathway by the regulation of PUMA expression by miR-144-3p. In conclusion, the new function of PUMA, PUMA on FDX1 and a novel approach to target PUMA were identified in our study, providing new therapeutic strategies for CRC.

Supplementary Information The online version contains supplementary material available at https://doi.org/10.1007/s13402-025-01093-2.

Acknowledgements We would like to thank the Analytical Instrumentation Center of Hunan University for providing assistance with the experimental instruments.

Author contributions YJ Z, FW, LL Z, GY J conceived and designed the experiments. The manuscript was written through the contributions of all authors, written by GY J mainly. JH L, ND, MM J, NN L, XX J were responsible for extracting data, analyzing data and interpreting results. GZ, XX T and YK were contributed to the design of the review protocol and interpreting results. All authors have given approval to the final version of the manuscript.

Funding We would like to thank the support of the Natural Science Foundation of Hunan Province (2025JJ50124, 2024JJ5526), the National Natural Science Foundation of China (82273172), the Shanghai Oriental Talent Program (BJWS2024032), the Shanghai Academic/Technology Research Leader (23XD1433000), the Postdoctoral Fellowship Program of CPSF (GZC20230773), the China Postdoctoral Science Foundation (2025M773937), and the Development of New Technologies for the Detection of Biomarkers in Colorectal Cancer (H202391469289).

Data availability No datasets were generated or analysed during the current study.

Declarations

Ethics approval and consent to participate Animal experiments were conducted under the permission and supervision of Hunan University Animal Use and Care Committee (Changsha, Hunan, China, SYXK2018-0006).

Consent for publication All authors agreed on the manuscript.

Competing interests The authors declare no competing interests.

References

1. H. Brenner, T. Heisser, R. Cardoso et al., Reduction in colorectal cancer incidence by screening endoscopy. Nat. Rev. Gastroenterol. Hepatol. **21**(2), 125–133 (2024)
2. L. Yang, J. Yang, A. Kleppe et al., Personalizing adjuvant therapy for patients with colorectal cancer. Nat. Rev. Clin. Oncol. **21**(1), 67–79 (2024)
3. M.W. Dougherty, C. Jobin, Intestinal bacteria and colorectal cancer: etiology and treatment. Gut Microbes. **15**(1), 2185028 (2023)
4. Y. Liu, H.C. Lau, W.Y. Cheng et al., Gut Microbiome in colorectal cancer: clinical diagnosis and treatment. Genomics Proteom. Bioinf. **21**(1), 84–96 (2023)
5. R.L. Siegel, K.D. Miller, H.E. Fuchs et al., Cancer statistics, 2022. CA Cancer J. Clin. **72**(1), 7–33 (2022)
6. D.L. Tang, G. Kroemer, R. Kang, Targeting Cuproplasia and Cuproptosis in cancer. Nat. Rev. Clin. Oncol. **21**(5), 370–388 (2024)
7. J. Wang, T. Ma, M. Wei et al., Copper in grape and wine industry: source, presence, impacts on production and human health, and removal methods. Compr. Rev. Food Sci. Food Saf. **22**(3), 1794–1816 (2023)

8. C.H. Lin, Y. Chin, M. Zhou et al., Protein lipoylation: mitochondria, cuproptosis, and beyond. Trends Biochem. Sci. **49**(8), 729–744 (2024)
9. V.N. Kim, MicroRNA biogenesis: coordinated cropping and dicing. Nat. Rev. Mol. Cell. Biol. **6**(5), 376–385 (2005)
10. M. Marzec, MicroRNA: a new signal in plant-to-plant communication. Trends Plant. Sci. **27**(5), 418–419 (2022)
11. S.N. Guo, J.H. Li, J. Li et al., Regeneration and proliferation of cardiomyocytes and its MicroRNA regulatory mechanisms. Int. J. Dev. Biol. **66**(7–8–9), 359–372 (2022)
12. H.H. Genedy, P. Humbert, B. Laoulaou et al., MicroRNA-targeting nanomedicines for the treatment of intervertebral disc degeneration. Adv. Drug Deliv Rev. **207**, 115214 (2024)
13. B.T. Jones, J. Han, H. Zhang et al., Target-directed MicroRNA degradation regulates developmental MicroRNA expression and embryonic growth in mammals. Genes Dev. **37**(13–14), 661–674 (2023)
14. J. Li, S. Guo, Z. Sun et al., Noncoding RNAs in drug resistance of Gastrointestinal stromal tumor. Front. Cell. Dev. Biol. **10**, 808591 (2022)
15. M. Yuan, X. Zhang, F. Yue et al., CircNOLC1 promotes colorectal Cancer liver metastasis by interacting with AZGP1 and sponging miR-212-5p to regulate reprogramming of the oxidative Pentose phosphate pathway. Adv. Sci. (Weinh). **10**(33), e2205229 (2023)
16. C. Phetkong, C. Ariyachet, MicroRNAs in liver fibrosis: unraveling intercellular crosstalk and the regulatory functions of MicroRNA-223. BIOI, 2025, **6**(1)
17. H. Hermeking, The family in cancer and apoptosis. Cell. Death Differ. **17**(2), 193–199 (2010)
18. X. Lin, S. Wang, M. Sun et al., miR-195-5p/NOTCH2-mediated EMT modulates IL-4 secretion in colorectal cancer to affect M2-like TAM polarization. J. Hematol. Oncol. **12**(1), 20 (2019)
19. H. Ji, T.W. Kim, W.J. Lee et al., Two circPPFIA1s negatively regulate liver metastasis of colon cancer via miR-155-5p/CDX1 and HuR/RAB36. Mol. Cancer. **21**(1), 197 (2022)
20. Z. Rong, Z. Luo, Z. Fu et al., The novel circSLC6A6/miR-1265/C2CD4A axis promotes colorectal cancer growth by suppressing p53 signaling pathway. J. Experimental Clin. Cancer Res. **40**(1), 324 (2021)
21. Y. Zhang, D. Xing, L. Liu, PUMA promotes Bax translocation by both directly interacting with Bax and by competitive binding to Bcl-X L during UV-induced apoptosis. Mol. Biol. Cell. **20**(13), 3077–3087 (2009)
22. J. Yu, L. Zhang, P.U.M.A. No, No death: implications for p53-dependent apoptosis. Cancer Cell. **4**(4), 248–249 (2003)
23. Y. Hussain, H. Khan, T. Efferth et al., Regulation of Endoplasmic reticulum stress by hesperetin: focus on antitumor and cytoprotective effects. Phytomedicine. **100**, 153985 (2022)
24. L. Zhang, H. Wang, W. Li et al., Pazopanib, a novel multi-kinase inhibitor, shows potent antitumor activity in colon cancer through PUMA-mediated apoptosis. Oncotarget. **8**(2), 3289–3303 (2017)
25. L. Sun, Y. Huang, Y. Liu et al., Ipatasertib, a Novel Akt inhibitor, induces transcription factor FoxO3a and NF-κB Directly Regulates PUMA-dependent Apoptosis Cell Death Dis. **9**(9), 911 (2018)
26. Y. Huang, N. Liu, J. Liu et al., Mutant p53 drives cancer chemotherapy resistance due to loss of function on activating transcription of PUMA. Cell. Cycle **18**(24), 3442–3455 (2019)
27. Z. Wu, L. Hong, G. Luo et al., SIRT6 promotes autophagy through direct interaction with ULK1 and competitive binding to PUMA. Genes Dis. **10**(5), 1747–1750 (2023)
28. H. Wang, L. Zhang, X. Yang et al., PUMA mediates the combinational therapy of 5-FU and NVP-BEZ235 in colon cancer. Oncotarget. **6**(16), 14385–14398 (2015)
29. J. Chen, J. Zhong, Y. Liu et al., Purified vitexin compound 1, a new neolignan isolated compound, promotes PUMA-dependent apoptosis in colorectal cancer. Cancer Med. **7**(12), 6158–6169 (2018)
30. N. Liu, X. Jiang, G. Zhang et al., LncRNA CARMN m6A demethylation by ALKBH5 inhibits mutant p53-driven tumour progression through miR-5683/FGF2. Clin. Translational Med. **14**(7), e1777 (2024)
31. G. Zhang, W. Mi, C. Wang et al., Targeting AKT induced ferroptosis through FTO/YTHDF2-dependent GPX4 m6A methylation up-regulating and degradating in colorectal cancer. Cell. Death Discovery. **9**(1), 457 (2023)
32. J. Li, G. Luo, C. Zhang et al., In situ injectable hydrogel-loaded drugs induce anti-tumor immune responses in melanoma immunochemotherapy. Mater. Today Bio. **14**, 100238 (2022)
33. P. Tsvetkov, S. Coy, B. Petrova et al., Copper induces cell death by targeting lipoylated TCA cycle proteins. Science. **375**(6586), 1254–1261 (2022)
34. A. Janic, L.J. Valente, M.J. Wakefield et al., DNA repair processes are critical mediators of p53-dependent tumor suppression. Nat. Med. **24**(7), 947–953 (2018)
35. F. Liu, J. Chen, K. Li et al., Ubiquitination and deubiquitination in cancer: from mechanisms to novel therapeutic approaches. Mol. Cancer. **23**(1), 148 (2024)
36. J.W. Kang, Z. Zhan, G. Ji et al., PUMA facilitates EMI1-promoted cytoplasmic Rad51 ubiquitination and inhibits DNA repair in stem and progenitor cells. Signal. Transduct. Target. Therapy. **6**(1), 129 (2021)
37. Y. Du, X. Zhao, F. He et al., A Vacancy-Engineering Ferroelectric Nanomedicine for Cuproptosis/Apoptosis Co-Activated Immunotherapy. Advanced materials **36**(30): e2403253 (2024)
38. J. Xie, Y. Yang, Y. Gao et al., Cuproptosis: mechanisms and links with cancers. Mol. Cancer. **22**(1), 46 (2023)
39. Y. Chen, L. Zhang, K.A. Jones, SKIP counteracts p53-mediated apoptosis via selective regulation of p21Cip1 mRNA splicing. Genes & development. **25**(7), 701–716 (2011)
40. R. Hubaux, K.L. Thu, B.P. Coe et al., EZH2 promotes E2F-driven SCLC tumorigenesis through modulation of apoptosis and cell-cycle regulation. J. Thorac. Oncology: Official Publication Int. Association Study Lung Cancer. **8**(8), 1102–1106 (2013)
41. D. Zhang, K. Zaugg, T.W. Mak et al., A role for the deubiquitinating enzyme USP28 in control of the DNA-damage response. Cell. **126**(3), 529–542 (2006)
42. J. Zhao, Z. Xu, J. Xie et al., The novel lnc-HZ12 suppresses autophagy degradation of BBC3 by preventing its interactions with HSPA8 to induce trophoblast cell apoptosis. Autophagy. **20**(10), 2255–2274 (2024)
43. T.L. Lee, W.C. Shen, Y.C. Chen et al., Mir221- and Mir222-enriched adsc-exosomes mitigate PM exposure-exacerbated cardiac ischemia-reperfusion injury through the modulation of the BNIP3-MAP1LC3B-BBC3/PUMA pathway. Autophagy, 2024: 1–20
44. K. Matsubara, Y. Matsubara, Y. Uchikura et al., Pathophysiology of preeclampsia: the role of exosomes. Int. J. Mol. Sci., 2021, **22**(5)
45. M. Inui, G. Martello, S. Piccolo, MicroRNA control of signal transduction. Nat. Rev. Mol. Cell Biol. **11**(4), 252–263 (2010)
46. C. Ji, X. Guo, The clinical potential of Circulating MicroRNAs in obesity. Nat. Reviews Endocrinol. **15**(12), 731–743 (2019)
47. P. Xu, M. Guo, B.A. Hay, MicroRNAs and the regulation of cell death. Trends Genet. **20**(12), 617–6124 (2004)
48. S. Ghafouri-Fard, A. Abak, S.F. Talebi et al., Role of miRNA and lncRNAs in Organ Fibrosis and Aging, Biomed. Pharmacother. **143**, 112132 (2021)
49. X. Gao, H. Zhao, J. Liu et al., Enzalutamide sensitizes Castration-Resistant prostate Cancer to Copper-Mediated cell death. Adv. Sci. (Weinh). **11**(30), e2401396 (2024)

50. L. Sun, Y. Zhang, B. Yang et al., Lactylation of METTL16 promotes Cuproptosis via m(6)A-modification on FDX1 mRNA in gastric cancer. Nat. Commun. **14**(1), 6523 (2023)
51. M.T. Villanueva, Protein degradation reaches further out. Nat. Rev. Drug Discovery. **19**(9), 587 (2020)
52. Y. Feng, D.J. Klionsky, Receptors make the pathway choice for protein degradation. Autophagy. **13**(10), 1617–1618 (2017)
53. D.A. Cruz Walma, Z. Chen, A.N. Bullock et al., Ubiquitin ligases: guardians of mammalian development. Nat. Rev. Mol. Cell Biol. **23**(5), 350–367 (2022)
54. H. Xu, Z. Guo, M. Li et al., Copper-Based nanomaterials for Image-Guided Cancer therapy. BIOI, 2024, **5**(1)
55. S. Lu, Y. Li, Y. Yu, Glutathione-Scavenging Celastrol-Cu nanoparticles induce Self-Amplified Cuproptosis for augmented Cancer immunotherapy. Adv. Mater. **36**(35), e2404971 (2024)
56. J. Li, G. Zhang, Z. Sun et al., Immunogenic Cuproptosis in cancer immunotherapy via an in situ Cuproptosis-inducing system. Biomaterials. **319**, 123201 (2025)
57. Z. Guo, D. Chen, L. Yao et al., The molecular mechanism and therapeutic landscape of copper and Cuproptosis in cancer. Signal. Transduct. Target. Therapy. **10**(1), 149 (2025)